An Effective Approach to Instantaneous Rain Attenuation Frequency Scaling Using Single or Multiple Satellite Based Measurements

F. Capelletti, *Member, IEEE,* L. Luini, *Senior Member, IEEE*

***Abstract*— A novel frequency scaling methodology, termed Effective Instantaneous Frequency Scaling (EIFS), is proposed for the real-time prediction of rain attenuation affecting Earth-space communication links. This approach enables the estimation of rain attenuation at a target frequency by scaling concurrent measurements taken along the same path at one or more lower frequencies. Propagation data from three beacon frequencies—18.7, 39.6, and 49.5 GHz—collected at the Spino d'Adda ground station during the 1995-1996 ITALSAT experimental campaign, were used to evaluate the accuracy of the proposed model. The results demonstrate excellent prediction accuracy, both statistically (root mean square – RMS – of the percentage error approximately equal to 13%) and in terms of time series (RMS of the absolute error lower than 1 dB), making EIFS well-suited for the design and operation of adaptive Propagation Impairment Mitigation Techniques (PIMTs). Moreover, the application of EIFS with concurrent data from two frequencies provides highly accurate estimates of point rain rate time series, indicating its potential use for remote sensing applications as well.**

***Index Terms*— Frequency scaling, propagation impairment mitigation techniques, rain attenuation, remote sensing**

I. Introduction

Satellite communications (SatCom) are progressively shifting towards higher carrier frequencies to accommodate growing bandwidth demands and enhance the efficiency of onboard satellite equipment, including the use of smaller and lighter antennas. In this regard, SatCom systems are anticipated to soon operate in the Q/V-band (40-50 GHz) in addition to the traditional Ka-band (20-30 GHz). Furthermore, the W-band (75-110 GHz) is projected to represent the next phase in the evolution of SatCom technology [1].

At these frequencies, the impact of tropospheric gases, as well as falling and suspended hydrometeors such as rain and clouds, must be carefully considered when designing, operating, and optimizing Earth-space communication links [2],[3]. Among all tropospheric factors affecting the propagation of electromagnetic waves, rain plays a particularly significant role at frequencies above approximately 10 GHz, as it severely degrades link quality and substantially reduces system availability [4]. Consequently, precise knowledge of rain attenuation on Earth-space paths is critical for ensuring the reliability and performance of such communication systems.

To address this need, significant efforts have been made since the latter half of the 20th century to design and conduct propagation experiments, typically involving the measurement of power received from space-borne beacon signals at multiple ground stations. Notable and long-running experimental campaigns include the ITALSAT experiment (1991–2001), which utilized three concurrent beacon transmissions at 18.7, 39.6, and 49.5 GHz [5], and the ongoing Aldo Paraboni Alphasat Experiment (2014–present), employing two monochromatic signals at 19.7 GHz and 39.4 GHz [6]. The primary challenges of such experimental activities lie in their substantial costs and inherent complexity.

The propagation data collected through such experimental campaigns, along with ancillary meteorological data recorded at the receiver site, have been and continue to be used to develop and validate increasingly accurate prediction models. While various approaches have been proposed to predict rain attenuation, some models demonstrate superior accuracy, reliability, and applicability. Notably, rain attenuation Frequency Scaling (FS) models offer improved performance by estimating attenuation at a target frequency f_T based on measurements taken at a lower frequency f_L along the same link. The enhanced accuracy of FS models arises from their ability to leverage valuable information embedded in the measurements at f_L, such as the inhomogeneous distribution of rainfall along the propagation path and its microphysical properties, typically characterized by the so-called Drop Size Distribution (DSD) [7].

Furthermore, in comparison to statistical prediction models (e.g., [8],[9],[10]), certain FS models also provide real-time rain attenuation predictions at f_T, with the same level of accuracy shown when applied on statistical basis. These real-time predictions are essential for the design and implementation of Propagation Impairment Mitigation Techniques (PIMTs) at the ground segment, such as Adaptive Coding and Modulation (ACM) or Uplink Power Control (ULPC).

Among the most widely used FS models in the literature, some ([11]-[15]) are predominantly empirical, meaning they are specifically tailored to measurements collected in particular

F. Capelletti is with the Department of Electronics, Information and Bioengineering (DEIB), Politecnico di Milano, Milan, Italy (e-mail: francesco.capelletti@polimi.it).

L. Luini is with the Department of Electronics, Information and Bioengineering (DEIB), Politecnico di Milano, Milan, Italy (e-mail: lorenzo.luini@polimi.it).

locations and for fixed frequency pairs. In contrast, other methodologies aim for broader global applicability by relying on physically sound approaches and enabling instantaneous application [16],[17]. However, a significant limitation of such models is the requirement for local 1-minute integrated rainfall rate data, or even DSD data, collected concurrently with rain attenuation measurements at frequency f_L. This can be a considerable constraint, particularly in regions where experimental data collection is not actively conducted.

This contribution proposes an innovative frequency scaling methodology, hereinafter referred to as Effective Instantaneous x-Frequency Scaling (EIx-FS) model, aiming to predict rain attenuation along an Earth-space link in real time by utilizing only concurrent measurements at a lower frequency along the same link, thereby eliminating the need for local high-resolution rain sensors and long-term measurements. Additionally, the model features a flexible architecture that allows for gradual improvement in its predictive performance by incorporating an increasingly larger set of concurrent measurements, collected along the same path at different frequencies (all obviously lower than f_T). This is why the model acronym include "x-", which, as clarified in more detail in Section III, can be replaced by S- (Single-) or by D- (Dual-). Furthermore, as a byproduct of the devised FS approach, EIFS provides high-accuracy estimates of point rain rate time series. The accuracy of the proposed model is validated against the data collected during the 1995-1996 period at the receiving site in Spino d'Adda, Northern Italy, as part of the ITALSAT experimental campaign [5].

The work is organized as follows. Section II presents the experimental setup and the data processing. The EIFS model development and rationale are illustrated in Section III. Section IV deals with the testing and validation of the results achieved by the proposed model and, finally, conclusions and possible future developments are reported in Section V.

II. EXPERIMENTAL SETUP AND DATA PROCESSING

A. The ITALSAT Experiment at Spino d'Adda

The ITALSAT geostationary satellite experiment [5], which started in January 1991 and concluded in January 2001, permitted extensive experimental activities aimed at studying and assessing the impact of the troposphere on Earth-space signal propagation across the Ka, Q and V bands. The space-borne propagation payload included a unique set of beacon frequencies: 18.7, 39.6 and 49.5 GHz, transmitting with vertical (V), circular (C) and switched horizontal/vertical (H/V) polarization, respectively.

This contribution takes advantage of the co-polar signal measurements collected at the ground station of Spino d'Adda, near Milano (Northern Italy), at 37.7° elevation angle. Signals from the three beacons were collected using a 3.5 m diameter antenna equipped with de-icing and auto-tracking systems. The main characteristics of the space and ground segments are summarized in Table I ([18],[19]). Furthermore, since 1994, the ground station at Spino D'Adda has been equipped with a set of noise injection radiometers operating at 13.0, 23.8 and 31.65 GHz, to evaluate cloud integrated liquid water content and integrated water vapor content, which are essential for establishing the correct rain free attenuation level. Additionally, a co-located tipping bucket rain gauge was available to collect local rain rate intensity time series with a 1 sample/min time resolution. The availability of the rain sensor during the experimental campaign was nearly 100%. Furthermore, a suite of traditional meteorological instruments, including a thermometer, hygrometer, and barometer, was also utilized throughout the entire observation period.

For more detailed information on the ITALSAT experiment conducted in Spino d'Adda, the reader is referred to [20], which also includes the main results obtained from 7 years of data (1994-2000).

TABLE I
MAIN FEATURES OF THE ITALSAT SATELLITE AND OF THE GROUND STATION AT SPINO D'ADDA

	ITALSAT satellite	Spino d'Adda station
Beacon frequencies (GHz) and wave polarization	18.7 V 39.6 C 49.5 H/V	
EIRP (dBW)	24 to 30	-
Latitude	0°	45.4° N
Longitude	13.2° E	9.5° E
Altitude above sea level (km)	35863	0.084
Link elevation	-	37.7 °
Antenna diameter (m)	-	3.5
G/T (dB/K) at 18.7 GHz	-	25.0
G/T (dB/K) at 39.6 GHz	-	30.4
G/T (dB/K) at 49.5 GHz	-	28.6
Sampling rate (Hz)	-	1

B. Experimental Dataset and Data Processing

ITALSAT measurements are highly suited for the development and testing of FS methodologies, as they constitute the only database of this kind featuring three beacon frequencies. Specifically, this contribution examines data collected during the 1995-1996 biennium, as these years represent the least rainy and the rainiest periods, respectively, of the entire experimental set.

As a first step, the total atmospheric attenuation A_T (dB) was derived from the received beacon power P (dBW) in [21]. This was achieved by resorting to the co-located microwave radiometer (MWR), which allows estimating the total tropospheric attenuation in non-rainy conditions, A^{MWR} (dB): the procedure to derive A_T from P is properly detailed in [22]. Fig. 2 shows the Complementary Cumulative Distribution Functions (CCDFs) of the resulting total atmospheric attenuation A_T at the three beacon frequencies, for the data collected during the 1995-1996 biennium at Spino d'Adda.

Isolating the attenuation due to rain from the total attenuation time series is challenging. In this contribution, we resorted to the procedure outlined in [16], which, for the sake of clarity, is briefly summarized hereinafter. The attenuation due to rain and clouds, namely A_{RC} (dB), is isolated from A_T as follows:

$$A_{RC} = A_T - A_G^{ITU} \tag{1}$$

where A_G^{ITU} (dB) is the attenuation due to gases along the slant path. A_G^{ITU} can be evaluated by defining equivalent heights for oxygen and water vapor, namely h_O (km) and h_W (km). Consequently, the oxygen and water vapor specific attenuations, computed following the methodology in Annex 1 of Recommendation ITU-R P.676-13 [23], are multiplied by h_O and h_W to obtain the zenith path attenuation due to gases, which is subsequently scaled using the cosecant law. This is mathematically expressed as:

$$A_G^{ITU} = \frac{h_O\gamma_O + h_W\gamma_W}{\sin(\theta)} \tag{2}$$

where θ (deg) is the elevation angle. Local data of temperature T (K), total pressure p (hPa) and relative humidity RH (%) measured by the co-located meteorological sensors are required for the evaluation of the specific attenuation induced by oxygen and water vapor, γ_O (dB/km) and γ_{WV} (dB/km), respectively [23].

The cloud attenuation A_C (dB) and the rain attenuation A (dB) are obtained using the attenuation component separation methodology devised in [16], i.e.:

$$A_C = \begin{cases} R_{RC}A_{RC} & \text{if} \quad A_{RC} \le A_{RC}^{\max} \\ A_C^{\max} & \text{otherwise} \end{cases} \tag{3}$$

$$A = A_{RC} - A_C \tag{4}$$

where

$$R_{RC} = a\exp(-b\,A_{RC}) + (1-a)\exp(-c\,A_{RC}). \tag{5}$$

Table II lists the coefficients a, b, c in (5) and the values of $A_C^{\max}$ (dB) and $A_{RC}^{\max}$ (dB) in (3), associated with each operating frequency. The rationale behind the approach outlined in [16] is to maximize the statistical agreement of the cloud attenuation derived from local radiosonde observations (RAOBS) — to be used as reference — and from the beacon data according to the equations (1)-(5). The RAOBS data were collected at Milano Linate Airport, roughly 20 km from Spino d'Adda, with launches performed twice a day. Starting from the RAOBS vertical profiles of pressure, temperature and relative humidity, the liquid water content was first calculated using the TKK cloud detection algorithm [24], and, afterward, the cloud attenuation was obtained by means of the Liebe MPM93 mass absorption model [25]. As an example, Fig. 1 compares the two cloud attenuation CCDF at 49.5 GHz: the coefficients in Table II were obtained by maximizing the agreement between the curves, as so was done also for the other two beacon frequencies.

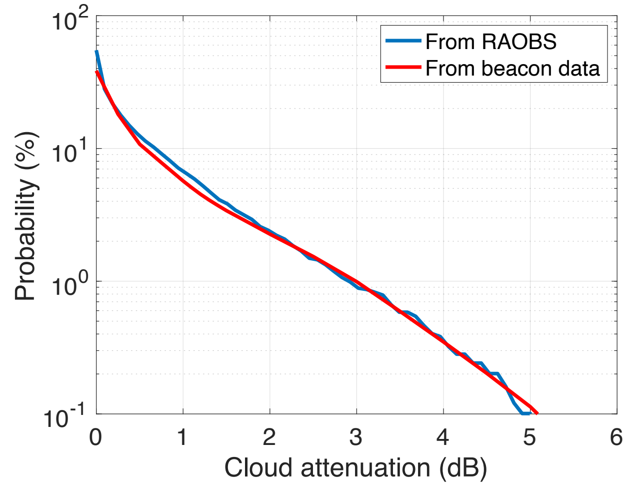

Fig. 1 CCDFs of the cloud attenuation at 49.5 GHz, obtained from RAOBS and from the beacon data using equations (1)-(5).

TABLE II
VALUES IN (3) AND COEFFICIENTS IN (5)

	a	b	c	$A_C^{\max}$	$A_{RC}^{\max}$
18.7 GHz	0.676	0.591	0.120	1.10	11.0
39.6 GHz	0.583	0.307	0.041	3.85	16.9
49.5 GHz	0.530	0.260	0.030	5.80	30.0

As a final step, the time series of A are averaged over 1-minute to achieve the same integration time as the co-located rain gauge.

The resulting CCDFs of the rain attenuation A for the considered biennium, evaluated at the three operating frequencies, are shown in Fig. 3. Such statistics are built from concurrent measurements: the joint beacon availability is reported in Table III.

To complete the description of the dataset used in this contribution, Fig. 4 illustrates the CCDF of the rain rate (mm/h) built from the data strictly concurrent with those used to produce the curves in Fig. 3. The overall probability to have rain at the site − $P_0^R = \Pr(R > 0 \text{ mm/h})$ − is 6.47%, while the probability of observing rain attenuation along the link − $P_0^A = \Pr(A > 0 \text{ dB})$ − is 8.71%.

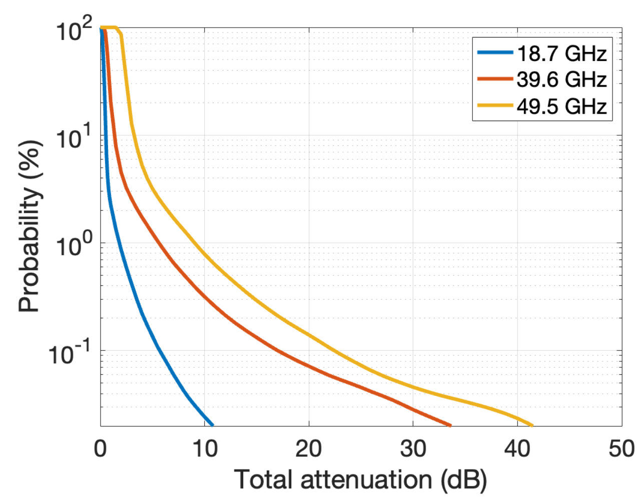

This article has been accepted for publication in IEEE Transactions on Antennas and Propagation. This is the author's version which has not been fully edited and content may change prior to final publication. Citation information: DOI 10.1109/TAP.2025.3552227

Fig. 2 CCDFs of the total attenuation at the three beacon frequencies, measured at the experimental ground station in Spino d'Adda (Northern Italy) for the 1995-1996 biennium.

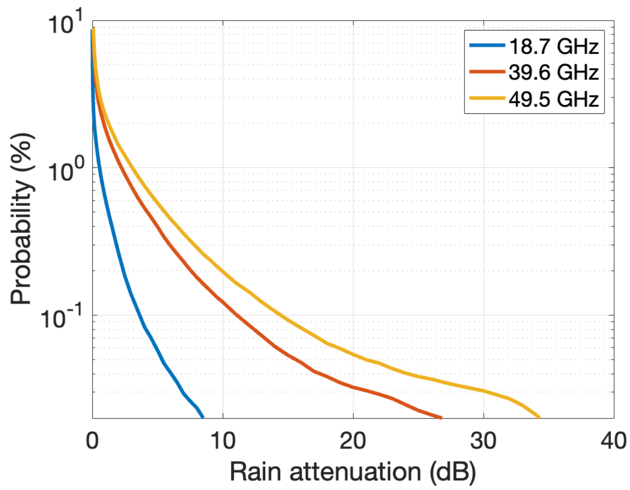

Fig. 3 CCDF of rain attenuation A at 18.7 GHz, 39.6 GHz, and 49.5 GHz, measured at Spino d'Adda and isolated from the total atmospheric attenuation A_T following the approach outlined in [16] and used in this contribution. Period: 1995 – 1996.

TABLE III
LINK AVAILABILITY FOR THE OBSERVATION PERIOD FROM 1995 TO 1996

	3 beacons	18.7 GHz	39.6 GHz	49.5 GHz
1995- 1996	87.5 %	97.2 %	88.9 %	95.5 %

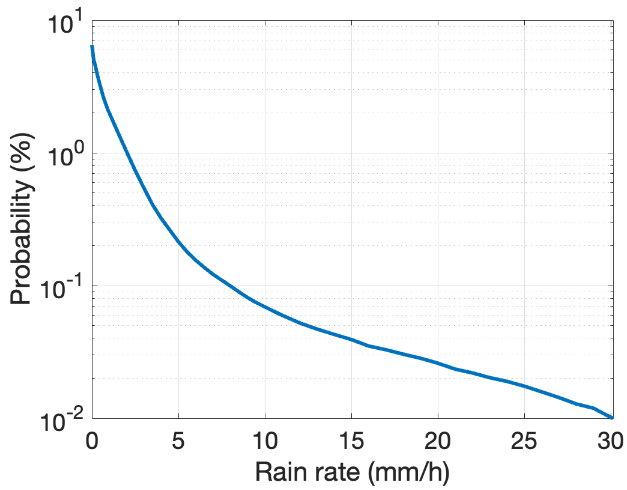

Fig. 4 CCDFs of the rain rate measured at the experimental ground station in Spino d'Adda (Northern Italy) for the 1995 – 1996 biennium.

As an example, Fig. 5 showcases the time series of A (top) and the concurrent rain rate R (bottom) for a convective event occurred on July 2, 1996, between approximately 9:30 UTC and 15:30 UTC. Though not easy to notice, the data show that, at the beginning of the event (around 9:45 UTC), $A > 0$ dB while the rain rate is very low (i.e., 0.2 mm/h): this indicates the presence of a rain cell along the path, which gradually approaches the ground station.

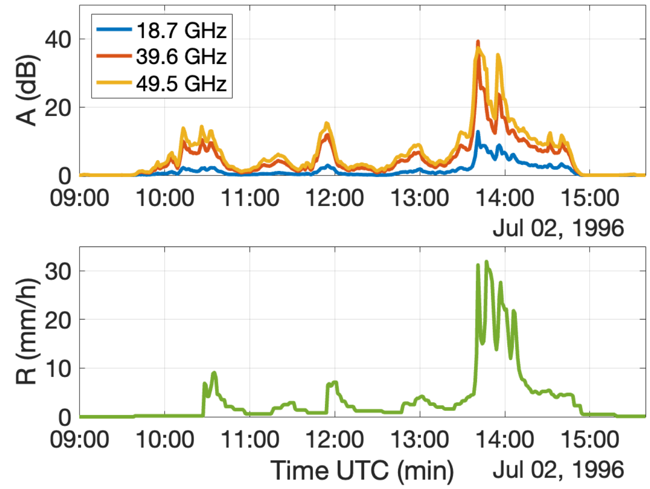

Fig. 5 Time series of rain attenuation A at 18.7 GHz, 39.6 GHz, and 49.5 GHz (top) and corresponding rain rate R (bottom) measured at Spino d'Adda on July 2, 1996.

III. FREQUENCY SCALING APPROACH: MODEL FORMULATION

The EIFS model, whose development and rationale is illustrated in this Section, relies on the physically based formulation of the rain attenuation A (dB) affecting an Earth-space link. Referring to the geometry depicted in Fig. 6, A can be estimated at a generic time t_0, as follows:

$$\tilde{A}(f, t_0) = \gamma_R(f, t_0)\, L_R\, PRF(t_0) \tag{6}$$

where $\gamma_R(f, t_0)$ (dB/km) represents the frequency-dependent specific rain attenuation at t_0, and L_R (km) is the portion of the link affected by rain, which extends from the ground up to h_R (km). The term PRF, or path reduction factor, accounts for the inhomogeneity of rain along the link, indicating that R (mm/h) is not uniform across the path [26]. Indeed, the concept of PRF is well-established and is utilized in several modeling approaches, for both terrestrial [27] and Earth-space links, including the most acknowledged one adopted in Recommendation ITU-R P.618-14 [15].

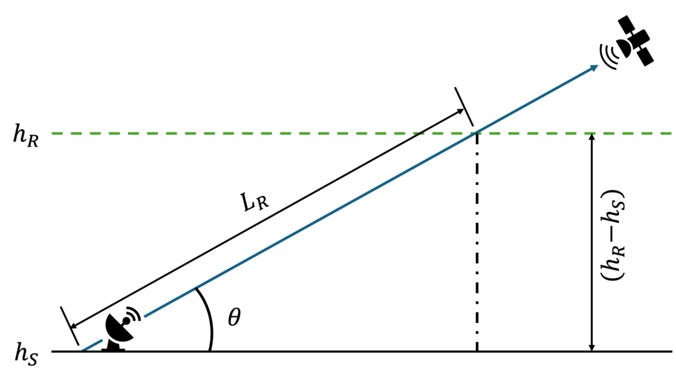

Fig. 6 Schematic presentation of the Earth-space link (blue line), highlighting the altitude of the ground station, h_S, the equivalent rain height, h_R, the elevation angle, θ, and the portion of the slant path below h_R, L_R.

γ_R can be expressed through the customary power-law relationship:

$$\gamma_R(f, t_0) = k(f)\, R(t_0)^{\alpha(f)} \tag{7}$$

where $R(t_0)$ is the rain rate (mm/h) measured at t_0, while k and α are coefficients tabulated in the Recommendation ITU-R P.838-3 as function of θ (deg), f (GHz), and wave polarization [28]. Though both coefficients depend on three parameters, from now on, for the sake of conciseness, only the dependence on f will be explicitly indicated. By means of simple geometrical considerations (please refer to Fig. 6), (6) becomes:

$$\tilde{A}(f, t_0) = k(f)\, R(t_0)^{\alpha(f)}\, \frac{(h_R(t_0) - h_S)}{\sin(\theta)}\, PRF(t_0) \tag{8}$$

The Effective Instantaneous Single-Frequency Scaling (EIS-FS) model relies on an instantaneous multiple-variable constrained optimization problem, receiving as input information on rain attenuation at only one lower frequency. The time-dependent objective function ϵ_S, evaluated at a generic time t_0, is defined as follows:

$$\epsilon_S(f_L, t_0) = \left|A(f_L, t_0) - \tilde{A}(f_L, t_0)\right| \tag{9}$$

where $A(f_L, t_0)$ denotes the measured rain attenuation, and $\tilde{A}(f_L, t_0)$ represents the physical-based expression of rain attenuation as in (8), both evaluated at the reference frequency f_L (GHz). As is clear from (8), the objective function ϵ_S depends on three unknowns, all of which could be potentially determined by the minimization algorithm: the point instantaneous rain rate (measured at the ground station), the instantaneous value of the path reduction factor, and the rain height, which, as indicated in (8), also changes with time. While the first two elements are expected to show a fast variability with time (orders of 1 minute), being both related to the space-time evolution of the rainfall process, the last one has a somewhat more limited dependence on t_0. This is clearly an underdetermined problem, whose solution becomes more cumbersome as the number of unknowns increases. In the attempt of reducing its complexity, in this contribution, $h_R(t_0)$ will be taken from ancillary meteorological information (more details provided in Section IV), thus becoming $\bar{h}_R$. Even so, the problem is still underdetermined; however, the definition of proper boundaries to the $R(t_0) - PRF(t_0)$ searching space are expected to provide accurate solutions.

For each time instant t_0, the optimization problem aims to determine the optimum values for the frequency-independent parameters $R(t_0)$ and $PRF(t_0)$, denoted as $R_{opt}(t_0)$ and $PRF_{opt}(t_0)$, by minimizing the objective function ϵ_S, as defined in (9). This minimization is subject to constraints that define the validity ranges for the two optimization variables, namely $\bar{R} = (R_L, R_U)$ and $\overline{PRF} = (PRF_L, PRF_U)$ for R and PRF, respectively. An initial starting point is assumed, denoted as $x_0 = (R_0, PRF_0)$. Such optimization problem can be mathematically translated into:

$$\min_{R,\,PRF} \epsilon_S(f_L, t_0)$$

$$\text{s.t.} \quad R_L < R(t_0) < R_U \tag{10}$$

$$PRF_L < PRF(t_0) < PRF_U.$$

If rain attenuation measurements are available at two reference frequencies, f_{L1} (GHz) and f_{L2} (GHz), the EIS-FS model can be easily extended to EID-FS. In this case, the objective function ϵ_D is:

$$\epsilon_D(f_{L1}, f_{L2}, t_0) = \epsilon_S(f_{L1}, t_0) + \epsilon_S(f_{L2}, t_0) = \left|A(f_{L1}, t_0) - \tilde{A}(f_{L1}, t_0)\right| + \left|A(f_{L2}, t_0) - \tilde{A}(f_{L2}, t_0)\right| \tag{11}$$

The new optimization problem becomes:

$$\min_{R,\,PRF} \epsilon_D(f_L, t_0)$$

$$\text{s.t.} \quad R_L < R(t_0) < R_U \tag{12}$$

$$PRF_L < PRF(t_0) < PRF_U.$$

The final step of the rain attenuation up-scaling process consists in applying (6) by incorporating the target frequency f_U (GHz), and the resulting $R_{opt}(t_0)$ and $PRF_{opt}(t_0)$ found from (10) or (12):

$$\tilde{A}(f_U, t_0) = k(f_U)\, R_{opt}(t_0)^{\alpha(f_U)}\, \frac{(\bar{h}_R - h_S)}{sin\,(\theta)}\, PRF_{opt}(t_0) \tag{13}$$

IV. EVALUATION OF MODEL PERFORMANCE

The accuracy of EIS-FS and EID-FS was tested by comparison with the measurements collected in the framework of the ITALSAT experimental campaign, specifically by using the A values described in Section II.B. More in detail, the following frequency scaling tests were performed:

a) EIS-FS from 18 GHz to 39 GHz;
b) EIS-FS from 18 GHz to 49 GHz;
c) EIS-FS from 39 GHz to 49 GHz;
d) EID-FS from 18 plus 39 GHz to 49 GHz.

In addition, when applying EIS-FS, two others prediction models are included in the statistical comparison: the model proposed by Drufuca in [29] and the model adopted in Section 2.2.1.3.2 of Recommendation ITU-R P.618-14 [15].

From a computational standpoint, the constrained optimization problems presented in Section III were solved using the MATLAB function *fmincon*, a nonlinear programming solver capable of finding the minimum of constrained multivariable functions. Specifically, *fmincon* was applied to the measured dataset on a minute-by-minute basis, with the following setup:

1. $\bar{R} = (R_L, R_U) = (0.1, 300)$ mm/h;

2. $\overline{PRF} = (PRF_L, PRF_U) = (0.5,1.5)$;
3. Starting point $x_0 = (R_0, PRF_0) = (5, 0.9)$;
4. Tolerance $T = 10^{-5}$ as stopping criteria.

While the choice for $\bar{R}$ is quite obvious, it is worth adding some words on $\overline{PRF}$. First, indications that PRF can be both lower and higher than 1 were drawn from [30], which includes an extensively analysis of *PRF*. The analysis was conducted for terrestrial links, but it is valid also for Earth-space links: in fact, the most relevant contribution to *PRF* is definitely given by the horizontal spatial correlation of the rain rate *R*, as the change in *R* with height is quite limited. The specific *PRF* lower and upper bounds, 0.5 and 1.5, respectively, were chosen by aiming at the compromise between: taking into account a sufficiently large range for *PRF*, for it to account for various possible rainy conditions along the link; limiting the optimization algorithm search space, for a quicker and more precise solution. Indications that the former point above is satisfied are inherently given by the good results obtained by EIFS, as explained in more detail below in this Section.

At this stage, a piece of information is still missing: $\bar{h}_R$ in (13) is calculated from the monthly mean values of the 0 °C isotherm height, in turn obtained from the ERA40 database produced by the European Center for Medium-Range Weather Forecasts (ECMWF) [31]. This choice represents a good compromise between employing data with higher temporal resolution (e.g. 1 hour) and using the more customary mean yearly value, typically used in rain attenuation prediction models. Fig. 7 illustrates the monthly trend of $\bar{h}_R$ at the site of Spino d'Adda for the biennium 1995-1996.

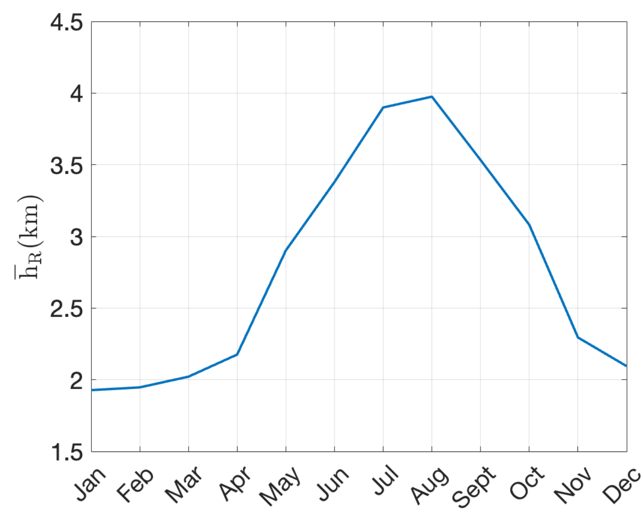

Fig. 7 Mean monthly trend of the equivalent rain height $\bar{h}_R$ (km) for the ground site of Spino d'Adda. Period: 1995-1996.

To more clearly and effectively discuss the results shown in Section IV, the following notation is introduced:

a) The measured rain attenuation at the channel frequency f will be denoted as A_f.
b) The measured rain rate will be denoted as R.
c) For the application of EIS-FS, the up-scaled rain attenuation will be denoted as $\tilde{A}_{f_L}^{f_T}$. The optimum rain rate, evaluated as in (10) at f_L, will be denoted as $\tilde{R}_{opt}^{f_L}$.
d) For the application of EID-FS, the up-scaled rain attenuation will be more simply denoted as $\tilde{A}_D^{f_T}$ (only one case is possible). The optimum rain rate, evaluated as in (12) at $f_{L1} + f_{L2}$, will be denoted as $\tilde{R}_{opt}^{D}$.
e) For the application of Drufuca, the up-scaled rain attenuation will be denoted as $\hat{A}_{f_L}^{f_T}$.
f) For the application of the ITU-R model, the up-scaled rain attenuation will be denoted as $\bar{A}_{f_L}^{f_T}$.

In all cases, the unit of f, f_L, f_{L1}, f_{L2}, f_T and R will be omitted, for the sake of conciseness.

Fig. 8, Fig. 9 and Fig. 10 show the results of the application of EIS-FS (full period). Specifically, Fig. 8 illustrates the comparison between the CCDFs of $A_{39.6}$ (blue) and $\tilde{A}_{18.7}^{39.6}$ (red). Fig. 9 and Fig. 10 depict the comparison for f_T = 49.5 GHz, using separately 18.7 GHz and 39.6 GHz, respectively, for f_L. The visual inspection of the results indicates that, while the Drufuca model is prone to overestimation, EIS-FS and the ITU-R model provide quite a satisfactory prediction accuracy across the entire probability range, both for f_T = 39.6 GHz and f_T = 49.5 GHz, the performance of the former being slightly worse than that of the ITU-R model. As expected, the prediction performance depends on the ratio $r = f_L/f_T$: the close is r to 1, the more accurate is the estimation.

The best results for EIFS are shown in Fig. 11, which reports the only case possible for the application of EID-FS: this is expected due to the dual information provided as input to the optimization problem.

The model's performance is quantified by employing the error figure defined in Recommendation ITU-R P.311-12 [32], typically employed to compare CCDFs of tropospheric attenuation. The error figure $\varepsilon(P)$ is expressed as:

$$\varepsilon(P) = \begin{cases} 100 \cdot \left(\frac{\tilde{A}(P)}{10}\right)^{0.2} \ln\left(\frac{A(P)}{\tilde{A}(P)}\right), \ \tilde{A}(P) < 10 \text{ dB} \\ 100 \cdot \ln\left(\frac{A(P)}{\tilde{A}(P)}\right), \ \tilde{A}(P) \geq 10 \text{ dB} \end{cases} \tag{14}$$

where $A(P)$ and $\tilde{A}(P)$ represents rain attenuations, both evaluated at the same probability level P, extracted from the measured and the estimated CCDFs, respectively. The resulting average (E) and root-mean-square (RMS) values of $\varepsilon(P)$ are listed in Table IV and Table V, respectively, confirming the considerations expressed above.

TABLE IV
OVERALL PREDICTION ACCURACY: AVERAGE (E) VALUES OF THE ERROR FIGURE IN (14)

	E (%)					
f_T / f_L	**39 GHz**			**49 GHz**		
18 GHz	10.48	14.69	6.14	19.82	29.45	10.32
39 GHz	-	-	-	8.91	14.65	2.13
18+39 GHz	-	-	-	7.62	-	-
	EIFS	**Drufuca**	**ITU**	**EIFS**	**Drufuca**	**ITU**

This article has been accepted for publication in IEEE Transactions on Antennas and Propagation. This is the author's version which has not been fully edited and content may change prior to final publication. Citation information: DOI 10.1109/TAP.2025.3552227

TABLE V
OVERALL PREDICTION ACCURACY: ROOT-MEAN-SQUARE (RMS) VALUES OF THE ERROR FIGURE IN (14)

f_T / f_L	RMS (%) 39 GHz			RMS (%) 49 GHz		
18 GHz	11.88	17.79	8.92	23.05	35.16	14.28
39 GHz	-	-	-	14.33	18.32	8.26
18+39 GHz	-	-	-	13.41	-	-
	EIFS	**Drufuca**	**ITU**	**EIFS**	**Drufuca**	**ITU**

As the minimization problems formalized in (10) and (12) can be instantaneously applied with an average computational time of a few seconds on a standard PC, the proposed methodology is suitable for real-time applications, i.e. to support the operation of ULPC. In fact, the limitations to the real-time applicability of EIFS for ULPC do not lie in calculation time required for the solution of the minimization problems in (10) and (12), rather they depend on the ability of the system to sample the signal at an adequate rate (the rain intensity rate of change is in the order of tens of seconds).

Fig. 12 and Fig. 13 show two examples comparing the trend of the rain attenuation as measured and as predicted by the models. The two figures refer to a stratiform and a convective event, respectively; the first one occurred on September 2, 1996, and the second one on August 08, 1995. Both figures include directly the application of both EIS-FS (all cases) and EID-FS.

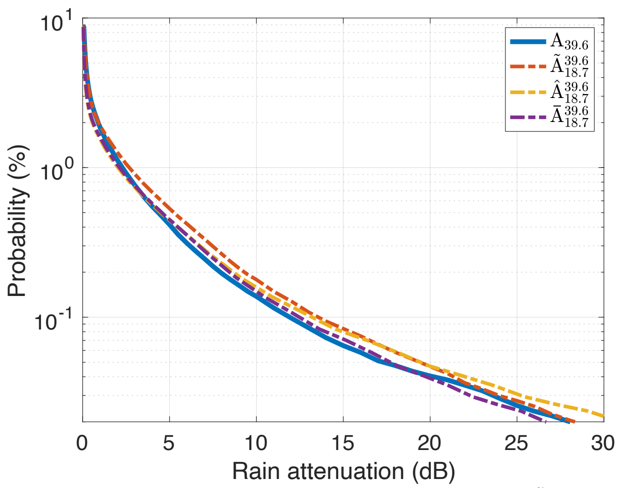

Fig. 8 Comparison between the CCDFs of $A_{39.6}$ (blue), $\tilde{A}_{18.7}^{39.6}$ (red), the Drufuca model $\hat{A}_{18.7}^{39.6}$ (yellow), and ITU-R model $\bar{A}_{18.7}^{39.6}$ (purple) for the Spino d'Adda ground site. Period: 1995-1996.

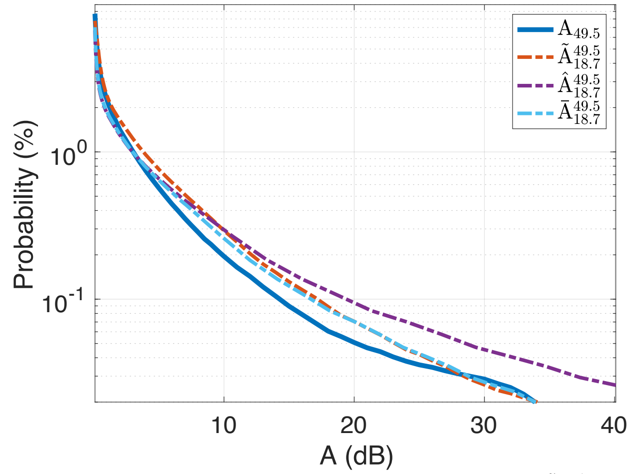

Fig. 9 Comparison between the CCDFs of $A_{49.5}$ (blue), $\tilde{A}_{18.7}^{49.5}$ (red), the Drufuca model $\hat{A}_{18.7}^{49.5}$ (purple) and the ITU-R model $\bar{A}_{18.7}^{49.5}$ (light blue) for the Spino d'Adda ground site. Period: 1995-1996.

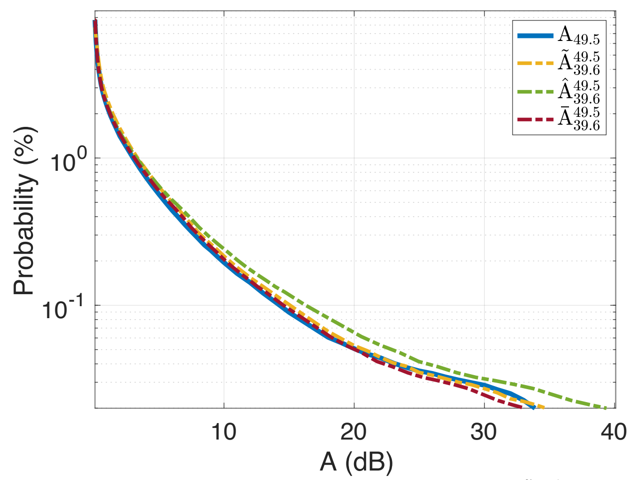

Fig. 10 Comparison between the CCDFs of $A_{49.5}$ (blue), $\tilde{A}_{39.6}^{49.5}$ (yellow), the Drufuca model $\hat{A}_{39.6}^{49.5}$ (green) and the ITU-R model $\bar{A}_{39.6}^{49.5}$ (burgundy) for the Spino d'Adda ground site. Period: 1995-1996.

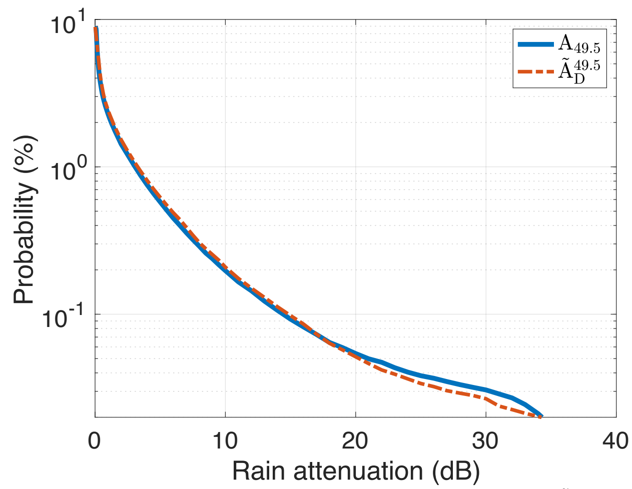

Fig. 11 Comparison between the CCDFs of $A_{49.5}$ (blue) and $\tilde{A}_{D}^{49.5}$ (red) for the Spino d'Adda ground site. Period: 1995-1996.

This article has been accepted for publication in IEEE Transactions on Antennas and Propagation. This is the author's version which has not been fully edited and content may change prior to final publication. Citation information: DOI 10.1109/TAP.2025.3552227

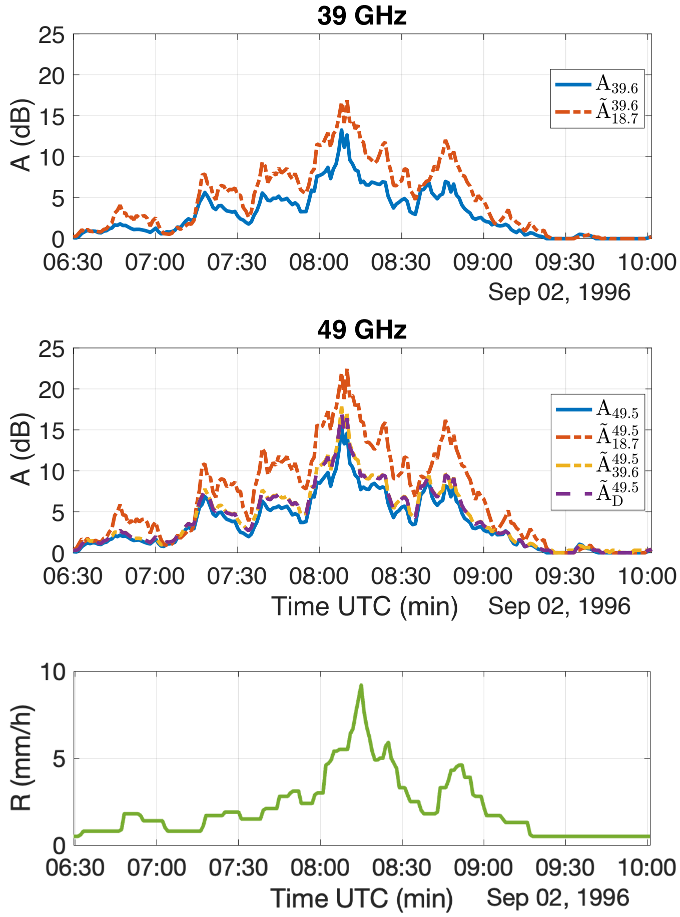

Fig. 12 Application of EIS-FS and EID-FS for f_T = 39.6 GHz (top) and f_T = 49.5 GHz (center), for a stratiform event (peak R < 10 mm/h) occurred on September 2, 1996, at Spino d'Adda. The concurrent rain rate is also reported (bottom).

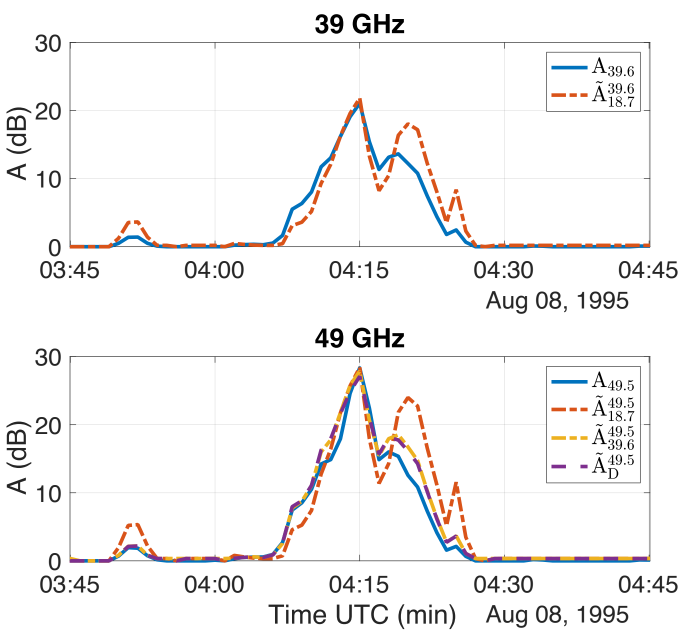

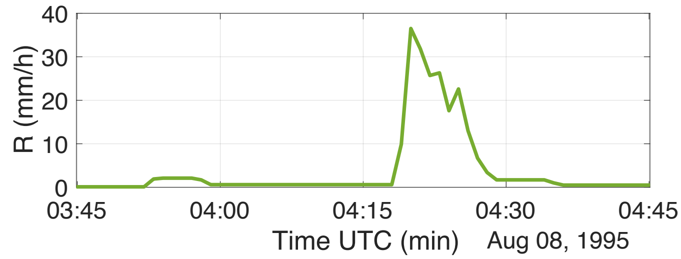

Fig. 13 Application of EIS-FS and EID-FS for f_T = 39.6 GHz (top) and f_T = 49.5 GHz (center), for a convective event (peak $R \geq$ 10 mm/h) occurred on August 08, 1995, at Spino d'Adda. The concurrent rain rate is also reported (bottom).

For the time series comparison, the prediction error is better quantified by E and RMS of the absolute error figure $\phi(t)$ (dB), defined as:

$$\phi(t) = A(t) - \tilde{A}(t) \tag{15}$$

where only samples for which $A(t) > 0$ are considered. The outcomes, for the whole 1995-1996 period, are listed in Table VI, remarking the significant accuracy provided by both the two scaling methods, i.e., EIS-FS and EID-FS, thereby indicating their potential usefulness for the application of fade mitigation techniques in fixed SatCom systems.

TABLE VI
OVERALL PREDICTION ACCURACY: AVERAGE (E) AND ROOT-MEAN-SQUARE (RMS) VALUES OF THE ABSOLUTE ERROR FIGURE IN (14). PERIOD: 1995-1996.

	E (dB)		**RMS (dB)**	
f_U / f_L	**39 GHz**	**49 GHz**	**39 GHz**	**49 GHz**
18 GHz	-0.11	-0.23	0.38	0.70
39 GHz	-	-0.22	-	0.37
18+39 GHz	-	-0.18	-	0.33

As is clear from the mathematical framework presented in Section III, the estimation of the optimal rain rate $\tilde{R}_{opt}$ (mm/h) is a byproduct of both EIS-FS and EID-FS. It is therefore worth comparing the time series of $\tilde{R}_{opt}$ with the ones of the rain rate measured by the rain gauge in Spino d'Adda. Fig. 14 compares the CCDFs of the rain rate as measured and as estimated for all the possible application cases: a) solution of (10) with f_L = 18.7 GHz; b) solution of (10) with f_L = 39.6 GHz; c) solution of (12) with f_{L1} = 18.7 GHz + f_{L2} = 39.6 GHz. The results clearly indicate that combining measurements at both frequencies – case c) – enhances the rain rate prediction accuracy.

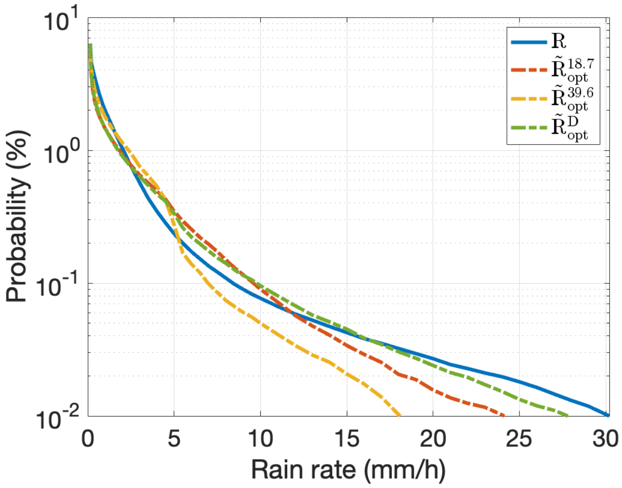

Fig. 14 CCDFs of the rain rate as measured and as estimated for all the possible application cases: a) solution of (10) with f_L = 18.7 GHz ($\tilde{R}^{18.7}_{opt}$); b) solution of (10) with f_L = 39.6 GHz ($\tilde{R}^{39.6}_{opt}$); c) solution of (12) with f_{L1} = 18.7 GHz + f_{L2} = 39.6 GHz ($\tilde{R}^{D}_{opt}$).

To quantify the prediction accuracy, a new error metric is defined, i.e.:

$$\varepsilon_r(P) = 100\frac{\tilde{R}_{opt}(P) - R(P)}{R_{opt}(P)} \tag{16}$$

evaluated at different probability levels P. Table VII lists the resulting E and RMS values for the three different optimization problems outlined above.

The same prediction accuracy can be observed on a temporal basis, as shown in Fig. 15 for two rain events, stratiform and convective, occurred on September 21, 1996, and October 15, 1996, respectively.

TABLE VII
OVERALL PREDICTION ACCURACY: AVERAGE (E) AND ROOT-MEAN-SQUARE (RMS) VALUES OF THE RELATIVE ERROR FIGURE

	E (%)	**RMS (%)**
18 GHz	-7.09	21.64
39 GHz	-23.14	34.28
18+39 GHz	6.02	13.46

V. CONCLUSIONS

This contribution proposes a novel frequency scaling methodology, suitable both for upscaling and downscaling, the former application being the most common one for the design and operation of typical SatCom links. Such approach, referred to as EIFS, aims to instantaneously predict rain attenuation at the target frequency f_T by leveraging concurrent measurements at one or potentially more frequencies $f_L < f_T$. The key advantages of this approach lie in its minimal input requirements: the rain attenuation at f_L and the mean monthly values of the equivalent rain height; indeed, no information on the rain rate is required. As a result, the instantaneous application of EIFS with relatively low computational time − few seconds − makes it particularly suited for the operation of PIMTs, such as ULPC, along any two-way SatCom link, be it a gateway (GW) link or a Very Small Aperture Terminal (VSAT) one. What changes between the two scenarios is how rain attenuation A can be estimated. For GW links, full knowledge of the equipment is expected and thus total tropospheric attenuation affecting the downlink can be in principle obtained by inverting the link budget equation. On the contrary, for VSAT links, full knowledge of the equipment is unlikely, but rain attenuation can still be obtained in real time from the received power using different approaches, such as the one proposed in [33].

The accuracy of EIFS, both utilizing data at one (EIS-FS) and two (EID-FS) input frequencies, was tested against the propagation data collected at Spino d'Adda (Northern Italy),

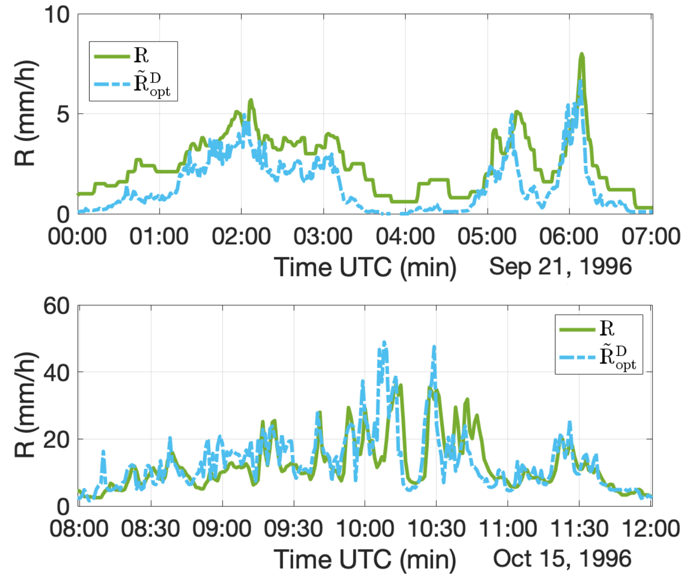

Fig. 15 Temporal comparison between the measured rainfall rate in Spino d'Adda (green) and as estimated from the solution of (12) with f_{L1} = 18.7 GHz + f_{L2} = 39.6 GHz; a stratiform event occurred on September 21, 1996 (top) and a convective event occurred on October 15, 1996 (bottom).

during the 1995-1996 biennium in the frame of the ITALSAT experimental campaign. Such a database is particularly valuable for testing EIFS, as it includes measurements from three concurrent beacon signals at 18.7, 39.6, and 49.5 GHz. The ITALSAT derived rain attenuation measurements were compared, both on a statistical and on a time series basis, against the predictions obtained by applying EIS-FS and EID-FS. Specifically, the following scenarios were investigated: a) EIS-FS from 18 GHz to 39 GHz, b) EIS-FS from 18 GHz to 49 GHz, c) EIS-FS from 39 GHz to 49 GHz, and d) EID-FS from 18 plus 39 GHz to 49 GHz.

Statistical scaling results at the target frequency of 39 GHz show satisfactory accuracy, yielding an RMS of the ITU-R defined error figure of 11.88%. Comparable accuracy was observed at 49 GHz: in this case, the resulting RMS provided by the EIS-FS – case c) – and the EID-FS is nearly halved compared to the RMS associated to EIS-FS – case b), decreasing from 23.05% to 14.33% and 13.41%, respectively. Though the performance on statistical basis of both EIS-FS and EID-FS is slightly worse than the one delivered by the model adopted in Recommendation ITU-R P.618-14 (Section

2.2.1.3.2), the key advantage of the proposed FS methodology lies in its increasing accuracy and soundness (building upon its physical basis) as the number of input frequencies grows: this feature opens the door to the application of EI-FS to obtain reliable predictions at frequency bands for which no (or very scares) data are currently available (e.g. W band).

A similar halving trend, statistically measured passing from EIS-FS to EI-FS, was observed on the tests conducted on time series.

As a byproduct, the optimal rain rate estimated by the EID-FS turns out to accurately reproduce the trend of the rainfall measurements collected by the local rain gauge. These outcomes suggest that EID-FS can be potentially used also in remote sensing applications, where local high-resolution values of the rain rate are required.

Future work includes testing EIFS on datasets collected in other sites, both for rain attenuation prediction and possibly for rain rate retrieval (depending on the number of input frequencies). Also, equivalent rain height measurements with increased time resolution (e.g. 1 hour) can be employed to verify if and to what extent this may lead to the further increase in the EIFS prediction accuracy.

REFERENCES

[1] M. Biscarini, G. Stazi, L. Milani, L. Luini, C. Riva, D. Cimini, S. Gentile, F. Romano, G. Brost and A. Martellucci. (2023, Sept.). Statistical modeling of atmospheric propagation channel at W-band through sun-tracking microwave radiometric measurements for non-geostationary satellite links. *IEEE Trans. Antennas Propag*. [Online]. *71 (9)*, pp. 7512-7522.

[2] C. Riva, C. Capsoni, L. Luini, M. Luccini, R. Nebuloni and A. Martellucci. (2013, Aug.). The challenge of using the W band in satellite communication. *Int. J. Satell. Commun. Network.* [Online]. *32 (3),* pp. 187-200.

[3] R. K. Crane, “Effects of Rain,” in *Electromagnetic Wave Propagation Through Rain,* New York, NY, USA: Wiley, 1996.

[4] J. E. Allnutt, “Satellite-to-Ground Radiowave Propagation,” 2nd Ed., The Institution of Engineering and Technology, 2011.

[5] F. Fedi, A. Paraboni, A. Martinelli and A. Martellucci. (1990). The ITALSAT program: the propagation experiment. *Rivista Tecnica Selenia. 32 (4),* pp. 40-59.

[6] T. Rossi, M. De Sanctis, M. Ruggieri, C. Riva, L. Luini, G. Codispoti, E. Russo, G. Parca. (2016, March). Satellite communication and propagation experiments through the alphasat Q/V band Aldo Paraboni technology demonstration payload. *IEEE Aerospace and Electronic Systems Magazine. 31 (3),* pp. 18-27.

[7] European Space Agency, “Propagation for SatCom services at Ku-band and above,” COST Action 255, Noordwijk, The Netherlands, 2002.

[8] L. Luini, C. Riva, C. Capsoni, and A. Martellucci (2007, July). Attenuation in non rainy conditions at millimeter wavelengths: assessment of a procedure. *IEEE Transactions on Geoscience and Remote Sensing. 45(7),* pp. 2150-2157.

[9] G. H. Bryant, I. Adimula, C. Riva, and G. Brussaard (2001). Rain attenuation statistics from rain cell diameters and heights. *Int. J. Satellite Commun. 19(3)*, pp. 263–283.

[10] A. Dissanayake, J. Allnutt, and F. Haidara (1997). A prediction model that combines rain attenuation and other propagation impairments along earth-satellite paths. *IEEE Trans. Antennas Propag. 45(10)*, pp. 1546–1558.

[11] F. Dintelmann, G. Ortgies, F. Rucker, and R. Jakoby. (1993, Jun). Results from 12-30 GHz German propagation experiments carried out with radiometers and the OLYMPUS satellite. *Proceedings of the IEEE. 81 (6)*, pp. 876–884.

[12] B. Segal, "Rain attenuation statistics for terrestrial microwave links in Canada," NASA STI/Recon Technical Report N 82, pp. 14–15. 1982.

[13] CCIR, "Attenuation by hydrometeors, in precipitation, and other atmospheric particles," CCIR Report 721-3, Propagation in Non-Ionized Media, pp. 5. Geneva. 1990.

[14] L. Boithias. (1986). Similitude en frequence pour l'affaiblissement par la pluie. *Ann. Telecommun. 44 (3–4)*, pp. 186–191.

[15] Propagation data and prediction methods required for the design of Earth-Space telecommunication systems, ITU-R P.618-14, 2023.

[16] L. Luini, A. Panzeri and C. Riva (2020, Mar.). Enhancement of the synthetic storm technique for the prediction of rain attenuation time series at EHF. *IEEE Trans. Antennas Propag.* [Online]. *68 (7)*, pp. 5592-5601.

[17] L. Luini, A. Panzeri, and C. Riva (2021, March). Frequency Scaling Model for the Prediction of Total Tropospheric Attenuation Time Series at EHF. *IEEE Transactions on Antennas and Propagation. 69(3)*, pp. 1569-1580.

[18] U. C. Fiebig and C. Riva. (2004). Impact of seasonal and diurnal variations on satellite system design in V band. *IEEE Transactions on Antennas and Propagation*, *52 (4),* pp. 923-932.

[19] R. Polonio and C. Riva. (1998). ITALSAT propagation experiment at 18.7, 39.6 and 49.5 GHz at Spino D'Adda: three years of CPA statistics. *IEEE transactions on antennas and propagation*, *46 (5)*, pp. 631-635.

[20] C. Riva. (2004). Seasonal and diurnal variations of total attenuation measured with the ITALSAT satellite at Spino d’Adda at 18.7, 39.6 and 49.5 GHz. *International Journal of Satellite Communications and Networking.* [Online]. *22 (4)*, pp. 449-476.

[21] R. Polonio and C. Riva. (1998). ITALSAT propagation experiment at 18.7, 39.6 and 49.5 GHz at Spino d’Adda: three years of CPA statistics. *IEEE Trans. Antennas Propag*. [Online]. *46 (5)*, pp. 631-635.

[22] L. Luini, C. Riva, R. Nebuloni, M. Mauri, J. Nessel, and A. Fanti, “Calibration and use of microwave radiometers in multiple-site EM wave propagation experiments,” in *Proc. 12th Eur. Conf. Antennas Propag. (EuCAP)*, London, U.K., 2018, pp. 1–5.

[23] Attenuation by atmospheric gases and related effects, ITU-R P.676-13, 2022.

[24] E. Salonen and S. Uppala, “New prediction method of cloud attenuation,” *Electron. Lett.*, vol. 27, no. 12, p. 1106, 1991.

[25] H. J. Liebe, G. A. Hufford, and M. G. Cotton, “Propagation modelling of moist air and suspended water/ice particles at frequencies below 1000 GHz,” in Proc. 52nd Specialists’ Meeting EM Wave Propag., Panel, Palma De Maiorca, Spain, 1993, pp. 3-1–3-10.

[26] C. Capsoni, F. Fedi and A. Paraboni. (1987, May). A comprehensive meteorologically oriented methodology for the prediction of wave propagation parameters in telecommunication applications beyond 10 GHz. *Radio Science. 22 (3),* pp. 387-393.

[27] F. Capelletti, C. Riva, G. Roveda and L. Luini. (2024, Feb.). The path reduction factor for the prediction of rain attenuation affecting short EHF terrestrial links. *IEEE Open Journal of Antennas and Propagation. 5 (1),* pp. 225-237.

[28] Specific attenuation model for rain for use in prediction methods, ITU-R P.838-3, 2005.

[29] G. Drufuca (1974). Rain attenuation statistics for frequencies above 10 GHz from rain gauge observations. *J. Rech. Atmos*., pp. 1–2, pp. 399–411.

[30] F. Capelletti, C. Riva, G. Roveda, L. Luini, “The Path Reduction Factor for the Prediction of Rain Attenuation Affecting Short EHF Terrestrial Links”, *IEEE Open Journal of Antennas and Propagation*, vol. 5, no. 1, Page(s): 225-237, February 2024.

[31] S. M. Uppala, et al. (2005). The ERA-40 re-analysis. *Quarterly Journal of the Royal Meteorological Society: A journal of the atmospheric sciences, applied meteorology and physical oceanography*. *131(612)*, pp. 2961-3012.

[32] Acquisition, presentation and analysis of data in studies of tropospheric propagation, ITU-R P.311-12, 2005.

[33] R. A. Giro, L. Luini, C. Riva, “Rainfall Estimation from Tropospheric Attenuation Affecting Satellite Links”, *Information* 2020, 11(1), 11 - Special Issue on "Satellite Communication at Ka and Q/V Frequency Bands".

Francesco Capelletti (Member, IEEE) was born in Italy in 1997. He received the B.S. degree in Engineering of Computing Systems and the M.S. degree in Telecommunication Engineering from Politecnico di Milano, Milan, Italy, in 2021 and 2023, respectively.

He is currently pursuing a Ph.D. in Information Technology at DEIB (Dipartimento di Elettronica, Informazione e Bioingegneria) of Politecnico di Milano. His main research studies cover the propagation of electromagnetic waves in terrestrial and non-terrestrial radio systems, particularly focused on interference analysis and frequency management within radio-frequency systems.

Mr. Capelletti is actively involved within ITU-R Study Group (SG) 3, providing support to standardization activities. He is also participating in the “Enhanced Alphasat Aldo Paraboni QV Band Test-Bed Configurations for Additional Experiments” (CALIBRATE) and the “MEO Ka band Propagation Campaign” (MEKaP) projects, commissioned by the European Space Agency (ESA).

Lorenzo Luini (Senior Member, IEEE) received the Laurea Degree (cum laude) in Telecommunication Engineering in 2004 and the Ph.D. degree in Information Technology in 2009 (cum laude) both from Politecnico di Milano, Italy.

He is currently an Associate Professor at DEIB (Dipartimento di Elettronica, Informazione e Bioingegneria) of Politecnico di Milano. His research activities are focused on electromagnetic wave propagation through the atmosphere, both at radio and optical frequencies. He has been involved in several European COST projects, in the European Satellite Network of Excellence (SatNEx), as well as in several projects commissioned to the research group by the European Space Agency (ESA), the USA Air Force Laboratory (AFRL) and the European Commission (H2020).

Lorenzo Luini authored 240 contributions to international conferences and scientific journals. He is Associate Editor of IEEE Transactions on Antennas and Propagation (TAP) and of International Journal on Antennas and Propagation (IJAP), member of the Italian Society of Electromagnetism, Chair of the Working Group “Propagation” of EurAAP (European Association on Antennas and Propagation) and Leader of Working Group “Propagation data calibration” within the AlphaSat Aldo Paraboni propagation Experimenters (ASAPE) group.